Edinburgh Research Explorer

Climate Model-Simulated Diurnal Cycles in HIRS Clear-Sky Brightness Temperatures

Climate Model–Simulated Diurnal Cycles in HIRS Clear-Sky Brightness Temperatures

IAN A. MACKENZIE AND SIMON F. B. TETT

The University of Edinburgh, Edinburgh, United Kingdom

ANDERS V. LINDFORS

The University of Edinburgh, Edinburgh, United Kingdom, and
Finnish Meteorological Institute, Helsinki, Finland

ABSTRACT

Clear-sky brightness temperature measurements from the High-Resolution Infrared Radiation Sounder (HIRS) are simulated with two climate models via a radiative transfer code. The models are sampled along the HIRS orbit paths to derive diurnal climatologies of simulated brightness temperature analogous to an existing climatology based on HIRS observations. Simulated and observed climatologies are compared to assess model performance and the robustness of the observed climatology.

Over land, there is good agreement between simulations and observations, with particularly high consistency for the tropospheric temperature channels. Diurnal cycles in the middle- and upper-tropospheric water vapor channels are weak in both simulations and observations, but the simulated diurnal brightness temperature ranges are smaller than are observed with different phase and there are also intermodel differences. Over sea, the absence of diurnal variability in the models' sea surface temperatures causes an underestimate of the small diurnal cycles measured in the troposphere.

The simulated and observed climatologies imply similar diurnal sampling biases in the HIRS record for the tropospheric temperature channels, but for the upper-tropospheric water vapor channel, differences in the contributions of the 24- and 12-hourly diurnal harmonics lead to differences in the implied bias. Comparison of diurnal cycles derived from HIRS-like and full model sampling suggests that the HIRS measurements are sufficient to fully constrain the diurnal behavior.

Overall, the results suggest that recent climate models well represent the major processes driving the diurnal behavior of clear-sky brightness temperature in the HIRS channels. This encourages further studies of observed and simulated climate trends over the HIRS era.

1. Introduction

Reliable records of global atmospheric temperature and composition are fundamental to our understanding of climate processes. In particular, the ability to simulate past and current observations including high frequency variability and longer term trends and feedbacks is a key metric of climate model performance and thus of the uncertainty in future climate projections. However, there are relatively few global and globally consistent measurement datasets extending back beyond the past two

decades against which simulations can be evaluated. One such record is provided by the series of High-Resolution Infrared Radiation Sounders (HIRS). HIRS instruments onboard the National and Atmospheric Administration polar-orbiting satellites have been measuring brightness temperatures from the earth's atmosphere since late 1978. Measurements are made in a range of channels (wavelengths) providing information on temperature, humidity, and ozone concentrations in various layers from the surface to stratosphere. The HIRS measurements thus make up a rare global dataset of vertically resolved atmospheric measurements taken over a period in excess of 30 years during which CO_2 levels have been steadily rising. Consequently, HIRS data have featured in a number of climate studies. The water vapor channels have received particular attention (Bates and

Corresponding author address: Ian A. MacKenzie, The University of Edinburgh, School of GeoSciences, Crew Building, The Kings Buildings, Edinburgh EH9 3JN, United Kingdom.
E-mail: iamack@staffmail.ed.ac.uk

Jackson 2001; Soden et al. 2002; Soden et al. 2005; Chung et al. 2011; Shi and Bates 2011) owing to the key role played by tropospheric, and especially upper-tropospheric, water vapor in the amplification of anthropogenic climate change via radiative feedback (e.g., Held and Soden 2000; Gettelman and Fu 2008; Sherwood et al. 2010).

However, in common with other long-term observing systems the HIRS record contains inhomogeneities; causes include intersatellite differences and changes in the instrumental spectral response function over the duration of a single mission. Here, we focus on another major uncertainty: the diurnal sampling biases that arise from different satellites in the NOAA series having different local overpass times and from the overpass time of individual satellites changing as the orbit drifts. Correcting for these temporal biases requires knowing the diurnal behavior of the brightness temperatures recorded in each instrument channel; this is essential for the derivation of reliable decadal trends from measurements made by multiple HIRS instruments. Previously, diurnal cycles simulated by climate models have been used to reduce assumed temporal biases in temperature data from the Microwave Sounding Units (Mears et al. 2003; Mears and Wentz 2005), and a diurnal correction based on climate model simulations has also been applied to the HIRS record (Jackson and Soden 2007). Jackson and Soden find that their model-derived corrections are consistent with the differences in HIRS brightness temperatures measured at two local times in the ascending and descending orbital modes. However, without corroborating observations of the full diurnal cycle, the overall fidelity of model-simulated diurnal cycles in brightness temperature, and thus the more general applicability of model-based corrections, is not easily gauged.

In this study, we exploit a new observational climatology of diurnal cycles in clear-sky brightness temperatures developed solely from HIRS measurements (Lindfors et al. 2011) to examine the performance of climate models in reproducing observed diurnal behavior. In addition to probing the validity of using climate models to correct diurnal biases in observational records, comparing simulations with observations also challenges model representations of the key physical processes contributing to the diurnal cycle in brightness temperature including radiative transfer and large-scale dynamics, and thus provides information on the more general model performance (Yang and Slingo 2001).

The Lindfors et al. (2011) dataset comprises a global monthly climatology of diurnal cycles in clear-sky brightness temperatures measured by HIRS between 2002 and 2007—a period when up to four instruments with different overpass times were operating concurrently, giving a good sampling of the diurnal range. Here we

replicate this observed climatology from climate model simulations. The model atmospheres are sampled along the orbit track to match the temporal and spatial pattern of the HIRS measurements of the real atmosphere before calculating, via a forward model, the brightness temperature in each HIRS channel implied by the modeled atmospheric profile at each measurement location. The simulated brightness temperatures are then subjected to the same temporal and spatial aggregating and processing that was applied to the HIRS measurements in order to generate a climatology of simulated diurnal cycles analogous to the observationally based climatology.

The core of the paper compares the simulated and observed climatologies to examine (i) how closely the model diurnal behavior resembles the observed behavior when similarly sampled (an evaluation of model performance) and (ii) how closely the diurnal cycles inferred from HIRS-like sampling of the model resemble the true diurnal cycles inferred from the fully sampled model—an evaluation of how closely the Lindfors et al. climatology is expected to reflect real atmospheric behavior.

2. Data, models, and methods

a. HIRS data

We use the climatology of diurnal cycles in HIRS clear-sky brightness temperatures developed by Lindfors et al. (2011). This is based on near-nadir measurements made between 2002 and 2007 from four satellites, *NOAA-14* to *NOAA-17*, all calibrated to *NOAA-12* to remove intersatellite biases. The HIRS data and the various channels are described by Shi et al. (2008) and Robel (2009) and summarized in Table 1. Each channel responds to a rather broad layer of the atmosphere according to its vertical weighting function (Li et al. 2000, Fig. 2). The CO_2 channels (chs.) 1 to 7 record the temperature profile from the stratosphere (ch. 1) to the lower troposphere (ch. 7), while ch. 8 is a window channel sensitive to the temperature of the surface and lowermost troposphere. Radiances in the channels sensitive to emissions from gases with nonfixed distributions, ch. 9 (ozone) and chs. 10–12 (water vapor), depend on both the species concentration and on the local temperature. Variability in the HIRS measurements in these channels can thus arise from changes in either quantity. For ch. 12 there was a marked shift in frequency between the *NOAA-14* and *-15* instruments lifting the peak of the weighting function to higher altitude and decreasing the brightness temperatures by up to ~8 K. The consequent large adjustment of the *NOAA-15* to *-17*

TABLE 1. Details of *NOAA-12* HIRS channels, including the approximate peak pressure of the weighting function (WF) for a tropical atmospheric profile.

Channel number	Central wavelength (μm)	WF peak (hPa)	Sensitivity
1	14.98	40	CO_2, T
2	14.70	60	CO_2, T
3	14.49	80	CO_2, T
4	14.20	300	CO_2, T
5	13.96	400	CO_2, T
6	13.65	700	CO_2, T
7	13.30	800	CO_2, T
8	11.11	Surface	CO_2, T
9	9.74	Surface, 30	O_3, T
10	8.17	900	H_2O, T
11	7.31	500	H_2O, T
12	6.76	300	H_2O, T

measurements to the *NOAA-12* base (Shi and Bates 2011) potentially increases the uncertainty in the observed diurnal climatology for this channel.

b. Climate models and simulations

The principal climate model used in the study is the atmospheric component of the Hadley Centre Global Environment Model version 2 (HadGEM2-A) (Collins et al. 2008, 2011), which is participating in the Coupled Model Intercomparison Project Phase 5 (CMIP5) (Jones et al. 2011). HadGEM2-A has a horizontal resolution of 1.875° longitude by 1.25° latitude with 38 terrain-following, height-based levels extending from the surface up to ~40 km with a vertical resolution greater than 100 m near the surface and 1 to 5 km in the stratosphere. Equivalent simulations were also performed with the Hadley Centre Atmospheric Model, version 3 (HadAM3) (Pope et al. 2000), an earlier generation Hadley Centre model with a somewhat coarser resolution: 2.5° latitude × 3.75° longitude with 19 hybrid pressure levels up to 5 hPa (~37 km) and approximately half the vertical resolution of HadGEM2-A. Diurnal cycles of outgoing longwave radiation (OLR) computed by HadAM3 have previously been compared with those measured by the Earth Radiation Budget Experiment and found to capture the main features of the observations, particularly over land but with some differences of detail (Smith et al. 2008).

Major changes between HadGEM2-A and HadAM3 include an entirely new dynamical core, a substantially revised treatment of cloud processes and microphysics, and a major upgrade to the mass flux convection scheme. Additionally, in HadGEM2-A the ozone profile used by the radiation scheme is adjusted to track the dynamically changing tropopause. The treatment of land surface processes also differs. HadGEM2-A uses version 2.2

of the Met Office Surface Exchange Scheme (MOSES) (Essery et al. 2003), which includes a tiled model of subgrid heterogeneity calculating separate surface temperatures, and radiative, heat, and other fluxes for each surface type within a grid box. HadAM3 uses MOSES version 1 (Cox et al. 1999), calculating a single surface energy balance for each grid box.

Full details of the differences between the HadGEM and HadAM series of models are described and tabulated by Johns et al. (2006) and Martin et al. (2006, Table 1). Using these two largely independent models in our study provides an indication of the extent to which simulated diurnal behavior is dependent on model configuration and parameterization.

Both models were run from January 2001 through December 2007 forced by observed monthly sea surface temperatures and sea ice extents taken from the Hadley Centre Sea Ice and Sea Surface Temperature dataset (HadISST) (Rayner et al. 2003). This allowed a 1-yr spinup prior to the analysis period starting in January 2002. Carbon dioxide and other long-lived greenhouse gases were fixed at 2005 levels (Solomon et al. 2007) while annually repeating, monthly- and zonal-mean, present-day climatologies were used for ozone and anthropogenic sulfate aerosols. All other forcings and boundary conditions were representative of the 2000s.

c. Model sampling

The difficulties of comparing traditional globally synchronous climate model output, typically saved at daily or lower frequency, with satellite observations are well known (Engelen et al. 2000). Here we adopt a model sampling strategy designed to replicate the HIRS clear-sky measurements as closely as possible. During model integration the full global, three-dimensional, instantaneous fields of temperature, humidity, and ozone, along with surface temperature and pressure and cloud fraction were output at hourly frequency. The stored output was then subsampled offline to mimic the along-track sampling patterns of the HIRS instruments onboard the *NOAA-14* to *NOAA-17* platforms, that is, the four instruments operating between 2002 and 2007. This subsampling required knowing (i) where an instrument was viewing at any given time and (ii) the cloudiness of the model profile at those locations. Effectively, the instruments were ''flown through'' the stored model atmospheres following orbital paths calculated from fixed values of satellite altitude, period, and inclination along with local equator crossing times that were updated monthly to account for observed drift in the orbits of the NOAA satellites. The model grid boxes being nadir-viewed by one or more of the four instruments

during the hour represented by each model output (irrespective of whether or not clear-sky measurements were taken) were identified and categorized as either cloudy or clear-sky depending on their modeled cloud fraction. Guided by earlier climate model simulations of HIRS radiances (Allan et al. 2003; Iacono et al. 2003), we deemed cloudy and discarded all grid boxes with cloud fraction greater than 0.4. Atmospheric profiles from the remaining clear-sky boxes were retained, labeled by instrument, and used to calculate simulated HIRS radiances. To create a simulated dataset analogous to the observed, only days for which intersatellite calibrated HIRS measurements were available for a given instrument, and which thus contributed to the Lindfors et al. (2011) climatology, were included in the HIRS-like sampling.

Inevitably, the temporal and spatial cloud distributions, and thus the distribution of clear-sky data, in the model atmospheres differ from that in the real atmosphere viewed by HIRS. However, the intention was not to pair model samples with individual HIRS measurements, but rather to develop a model climatology from multiyear data representative of the HIRS sampling pattern. The climatological averaging process also reduces discrepancies arising from the disparity between the size of the model grid boxes, $\sim$200 km $\times$ $\sim$140 km at the equator for HadGEM2-A, and the ground instantaneous field of view of HIRS, which is a circle of diameter $\sim$20 km at nadir. It is assumed that the single simulated brightness temperature, having no precision error, is comparable to the average of all, likely spatially autocorrelated, measurements made within that model grid box during a single satellite overpass. Temporally all HIRS measurements made within a grid box over the course of an hour are simulated by the instantaneous model state at the central time; this hourly binning of the simulated measurements somewhat displaces and coarsens the diurnal sampling resolution provided by the observations.

In addition to the HIRS-like sampling, the entire global, hourly clear-sky model fields for the full 2002 to 2007 period were also retained to enable investigation of the sensitivity of the results to the sampling pattern (section 4).

d. Calculation of simulated brightness temperatures

Model results are compared most directly with HIRS measurements by calculating equivalent HIRS brightness temperatures from the temperature and composition of the simulated atmosphere. This forward approach leads to a unique simulation of the top of the atmosphere radiance for each channel and atmospheric profile, combining information from the discrete model levels with the radiative properties of the atmosphere and the spectral characteristics of each channel. There is no need for the a priori assumptions of the state of the observed atmosphere that are required in inverting measured radiances into atmospheric profiles.

Brightness temperatures corresponding to the modeled atmospheric profiles were calculated using the RTTOV v9.3 radiative transfer code (Saunders et al. 1999; Matricardi et al. 2004; Matricardi 2009) called from the Cloud Feedback Model Intercomparison Project (CFMIP) Observation Simulator Package (COSP) (Bodas-Salcedo et al. 2011). The nadir-view top of the atmosphere radiance in HIRS chs. 1 to 12 was calculated from the model profiles of temperature, water vapor, and ozone along with the surface (skin) temperature and pressure at the location (grid box) of each simulated measurement. Temperatures and mixing ratios in the uppermost model level were assumed to extend unchanged to the top of the atmosphere. Channels 1 and 9 have some sensitivity to the atmosphere above the model top, but the weighting functions peak well within the model domain (Li et al. 2000) and the assumed constant profiles do not materially affect the results presented. Land emissivity was fixed at the RTTOV default value of 0.98 while sea emissivities were calculated by the Infrared Surface Emissivity Model (ISEM; Sherlock 1999) incorporated within RTTOV.

The spectral response functions (SRFs) of the HIRS channels, that is, the relative sensitivity to radiation of different wavelengths, vary somewhat between instruments. Here, all simulated brightness temperatures were calculated with the SRF of the *NOAA-12* instrument irrespective of the satellite making that notional measurement. Using a single SRF for all simulated measurements generates a dataset retaining the temporal biases of the multisatellite sampling pattern, but free from imposed instrumental bias. The *NOAA-12* SRF was chosen for consistency with the Lindfors et al. (2011) climatology derived from HIRS measurements all intersatellite calibrated to *NOAA-12*. The *NOAA-12* SRF was also used to calculate brightness temperatures from the full global, hourly clear-sky model fields.

To account for the effect of increasing atmospheric CO_2 on the HIRS record (Chung and Soden 2010a,b), the global CO_2 concentration used by RTTOV in the calculation of brightness temperature was increased linearly, by month, from 371 ppmv (January 2002) to 384 ppmv (December 2007).

e. Fitting the diurnal cycle

A monthly averaged global climatology of the diurnal behavior of the simulated brightness temperatures was

generated following the method used by Lindfors et al. (2011) for the HIRS measurements. All simulated measurements between 2002 and 2007 made in each model grid box were grouped by month and fitted to a second-order Fourier series, Eq. (1), by least squares regression:

$$T_b = a_0 + a_1 \cos\frac{\pi(t - t_1)}{12} + a_2 \cos\frac{2\pi(t - t_2)}{12}. \quad (1)$$

Here a_0 is the mean level of brightness temperature (T_b) and t is local time. The diurnal behavior is defined by the parameters a_1 and a_2, representing half of the peak-to-peak amplitude of the 24- and 12-hourly oscillations, respectively, and by their corresponding phases t_1 and t_2.

Grid squares without at least one clear-sky model profile in each quarter of the 24-h day were excluded from the fitting process. The result of this exercise is one value per month and channel of the a_{0-2} and t_{1-2} parameters for each sufficiently sampled grid square on the native model grid. In addition to the gridded data, zonally fitted values over land and sea were calculated by performing a single Fourier fit on all measurements at each latitude grouped by surface type. For a particular HIRS instrument each daily ascending or descending measurement at a given latitude is made at the same local time, so this aggregation leaves the temporal sampling of the diurnal cycle unchanged but increases the number of samples at each measured local time. Lindfors et al. (2011) show that improving the sampling in this manner reduces the uncertainty of the fit and helps resolve small amplitudes.

f. Sensitivity of the diurnal fit

In a preliminary analysis, brightness temperatures were calculated with RTTOV using the *NOAA-14* SRF with fixed CO_2 and taking HIRS-like sampled output from each model day between 2002 and 2007 when a particular HIRS instrument was operating, irrespective of whether measurements from that day and instrument had been used in the creation of the Lindfors et al. (2011) climatology. The resulting fits for individual grid boxes differed somewhat in detail from those to be presented here, but the global distribution of fits and the zonal and global averages were largely unchanged, indicating their robustness and insensitivity to small differences in processing and sampling.

3. HIRS-sampled model versus HIRS observations

a. Diurnal amplitudes

We begin by comparing the diurnal cycles of clear-sky brightness temperatures simulated from the climate
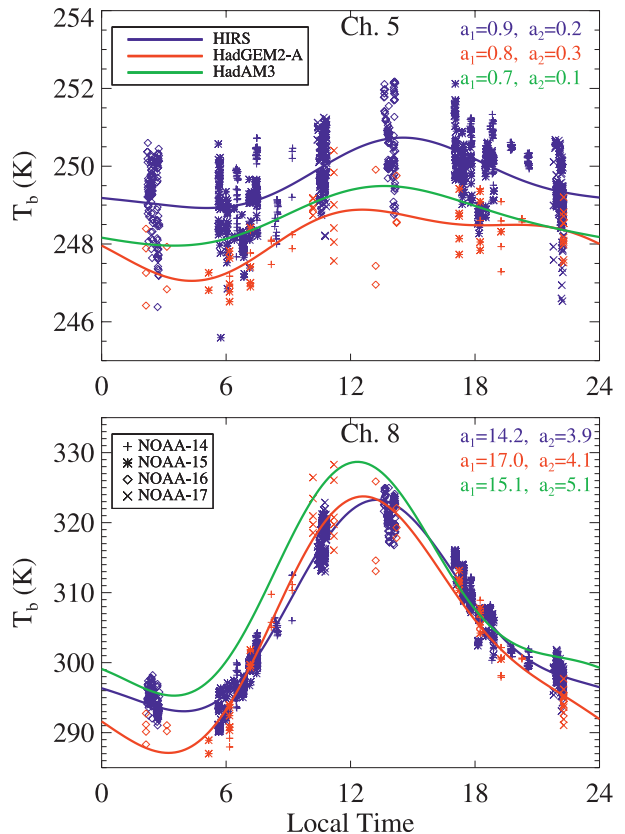

FIG. 1. Brightness temperatures in HIRS chs. 5 and 8 measured by HIRS and simulated from HadGEM2-A in July of 2002 to 2007 for the HadGEM2-A grid box centered on 31.25°N, 1.25°E. For HIRS each symbol represents a single measurement made within the grid box; for HadGEM2-A the symbols indicate the grid box value for the (hourly) output closest to the HIRS overpass time. The lines are the Eq. (1) Fourier fits to the data. The simulated fit for the 4× larger HadAM3 grid box centered on 30.0°N, 0.0° is shown without symbols. The numbers are the fit parameters a_1 and a_2. Lines and symbols are labeled on the top and bottom panels respectively. Note the different scales of the two y axes.

models when sampled like HIRS with the Lindfors et al. (2011) diurnal climatology inferred from the HIRS measurements themselves. This allows evaluation of the model ability to simulate real atmospheric behavior as seen by satellite. We compare the HIRS measurements and model simulations on a by-channel basis without deconvolving the sensitivities of each channel. The results obtained thus reflect the net performance of the climate model in reproducing all the processes driving the diurnal, and other, variability in that particular channel.

Figure 1 shows examples of diurnal fits from HIRS and HadGEM2-A for chs. 5 (midtropospheric temperature) and 8 (surface and lowermost tropospheric temperature) in a HadGEM2-A grid box over the Saharan desert, a region that is generally cloud free and thus well

sampled in both observations and simulations. The spread in the individual brightness temperatures measured or simulated at a particular local time is a reflection of the natural variability or "weather noise" in the real and model atmospheres over the six years for which data have been collected. This variability is expected to largely average out when taking a best fit through all the data points. The number of observed points exceeds the number simulated because, as already discussed, many individual measurements can be taken within the same model grid box during a single satellite overpass.

The diurnal cycles simulated from HadGEM2-A and observed by HIRS show similar behaviors: a strong cycle at the surface (ch. 8), and a weaker one in the middle troposphere (ch. 5), both dominated by the a_1 (diurnal or 24-hourly) harmonic. At the surface the simulated a_1 is somewhat larger than is observed, with the model being colder at night and having a steeper morning warming and evening cooling. In the midtroposphere the a_2 (semidiurnal or 12-hourly) harmonic makes a slightly larger contribution in the simulations than in the observations. There is also a small phase difference at both heights with the simulated brightness temperature peaking earlier in the afternoon. The 1-K to 2-K displacement of the HadGEM2-A and measured brightness temperatures in ch. 5 is consistent with a known cold bias in the extratropical troposphere of an earlier HadGEM model version (Martin et al. 2006). The fits from HadAM3, also shown in Fig. 1, are similar to those from HIRS and HadGEM2-A but are not directly comparable as they relate to a HadAM3 grid box four times larger than and somewhat displaced from the HadGEM2-A grid box.

Figure 2 shows the global distributions of the a_1 and a_2 harmonics for ch. 8 from the observations and simulations. Generally, both models closely resemble the observations, capturing the pronounced land–sea contrast and the occurrence of maxima in both harmonics over subtropical land areas and over high orography in the middle latitudes. The suppressed diurnal cycles in the strongly convecting intertropical convergence zones over equatorial Africa and South America are also captured, although the model amplitudes remain somewhat larger than the observations. The relative magnitude of the a_1 and a_2 harmonics over the continents is also well simulated by both models with the a_1 being generally ~3–4 times larger. In the desert regions of the subtropics, such as North Africa and the Arabian Peninsula, both harmonics tend to be slightly larger in HadGEM2-A than in HadAM3 and in the observations, consistent with the results seen for the Saharan grid box in Fig. 1. This may point to the version of the MOSES surface

exchange scheme used by HadGEM2-A producing overly dry desert soils, resulting in too large a sensible heat exchange with the atmosphere.

Over sea, the simulated amplitudes are mostly close to zero and, particularly for a_1, are markedly smaller than those observed. The almost flat diurnal cycles simulated for ch. 8 over sea are an expected consequence of the models being forced by a prescribed SST climatology having no daily variation. A Monte Carlo uncertainty analysis of the observations by Lindfors et al. (2011) finds that the HIRS a_2 values observed over sea, and shown here, are largely consistent with zero, but the observed HIRS a_1 values are significant above the noise level.

The greater spatial variability in the small amplitudes over sea in HadGEM2-A compared to HadAM3 likely stems from the finer horizontal resolution of HadGEM2-A. Persistent cloud causes the subantarctic region to be noisy and undersampled in both observation and simulations (more so in HadGEM2-A because there are fewer simulated measurements per grid box). HIRS and models also show a similar distribution of undersampled regions in the tropics and around Northern Hemisphere storm tracks. John et al. (2011) give further details on the availability of HIRS clear-sky data in convectively active tropical regions.

Qualitatively, the global distribution of ch. 8 a_1 from HadAM3 closely resembles the equivalent map of the diurnal cycle in all-sky OLR for northern summer calculated from the same model (Smith et al. 2008, Fig. 1b), consistent with the variation in OLR, on average, following that of the surface temperature.

Figure 3 compares a_1 and a_2 values zonally fitted over land for all channels from the HIRS observations and from the HadGEM2-A and HadAM3 simulations. A consistent picture emerges from the observations and both simulations with the amplitudes peaking for ch. 8 in the low and middle latitudes of both hemispheres, but more strongly in the summer, and with a pronounced tropical minimum, which is somewhat underrepresented (i.e., values remain too large) in the simulations, particularly for a_2. The same zonal distribution persists with weakening intensity in the other temperature channels on ascending the troposphere from channels 7 to 4. For both models the simulated ch.-4 a_2 amplitudes are consistently smaller than are observed, as is evident in the HadGEM2-A/HIRS ratio plot included in Fig. 3. Although ch. 4 has a rather broad weighting function, the distinct behavior compared to other channels with overlapping sensitivities suggests that the bias in the simulated a_2 amplitudes originates around the midtropospheric peak of the ch.-4 weighting function.

Solar heating by ozone absorption leads to a large diurnal cycle in the upper-tropospheric and stratospheric
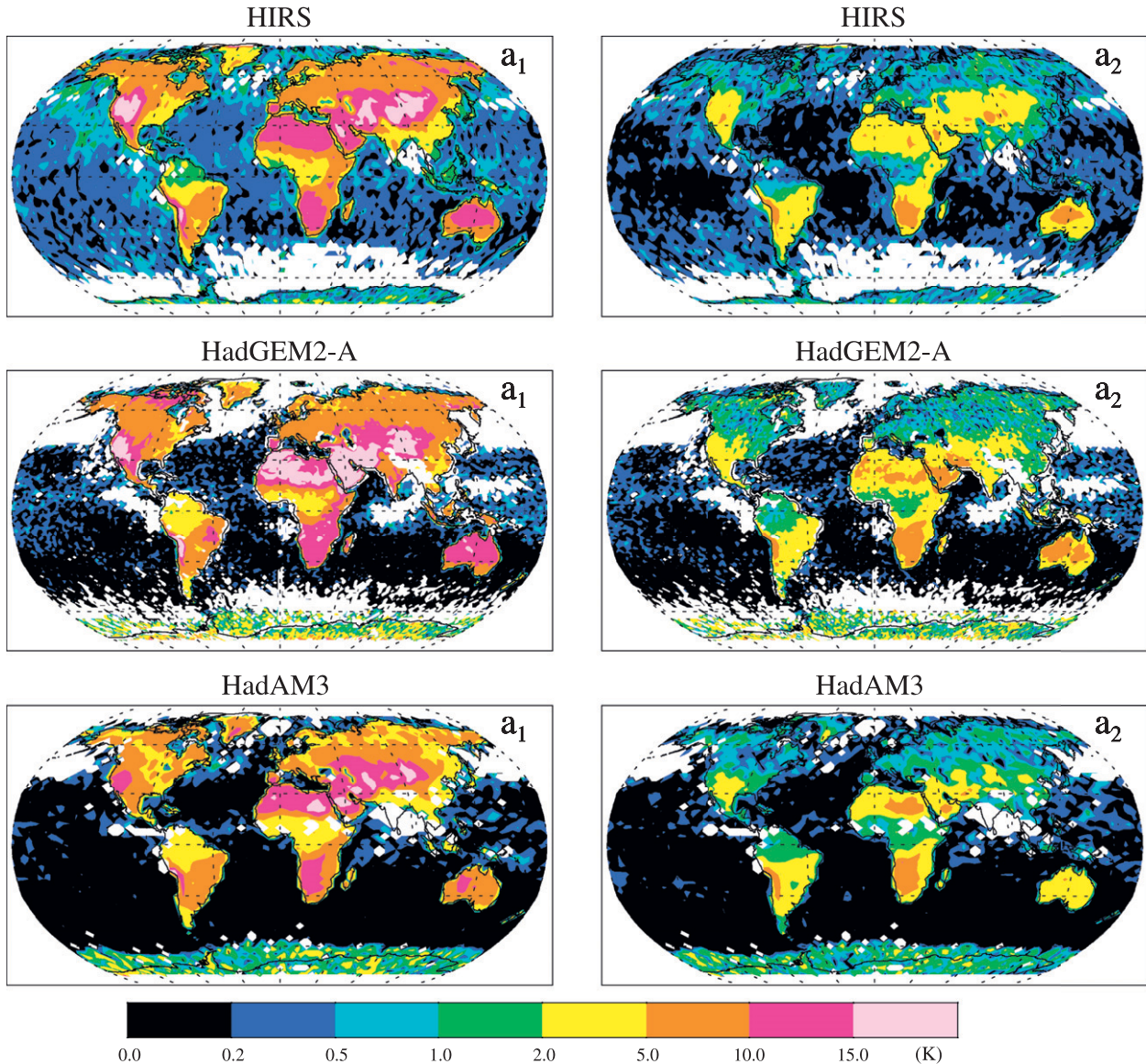
FIG. 2. Maps of the diurnal fit parameters a_1 and a_2 [see Eq. (1)] for ch. 8 brightness temperatures for July from the HIRS observations and from the HadGEM2-A and HadAM3 simulations. The HIRS observations are on a 2.5° × 2.5° grid while the simulations are on the native model resolutions. White shading indicates regions of insufficient clear-sky sampling.

temperature channels (3 to 1). A broad stratospheric maximum in a_1 centered on the summer subtropical/ middle latitudes occurs in the observations and in both simulations, but with greater intensity in HadGEM2-A than in HadAM3, which looks more like the observations. This apparent overestimate of the strength of the stratospheric diurnal cycle in HadGEM2-A is probably a consequence of the ozone scheme used by that model (see Fig. 5 and discussion). Lindfors et al. (2011) note that the amplitude of the diurnal cycle in the ch.-1 HIRS data is similar to that found in radio occultation data at around 30 km (Zeng et al. 2008).

The simulated amplitudes for chs. 9 (ozone) and 10 (lower-tropospheric water vapor) also closely follow the observations, showing a similar spatial distribution to the surface channel 8. Thus, aside from the aforementioned model underestimate of the tropical minimum, there is quantitative agreement, particularly in a_1, between simulations and observations for all channels from 4 to 10. The model overestimate of the tropical amplitudes may be due at least in part to sampling issues related to cloud filtering. HIRS with its ~20 km field of view can see small clear-sky regions of suppressed diurnal cycle in the vicinity of convective clouds, whereas all
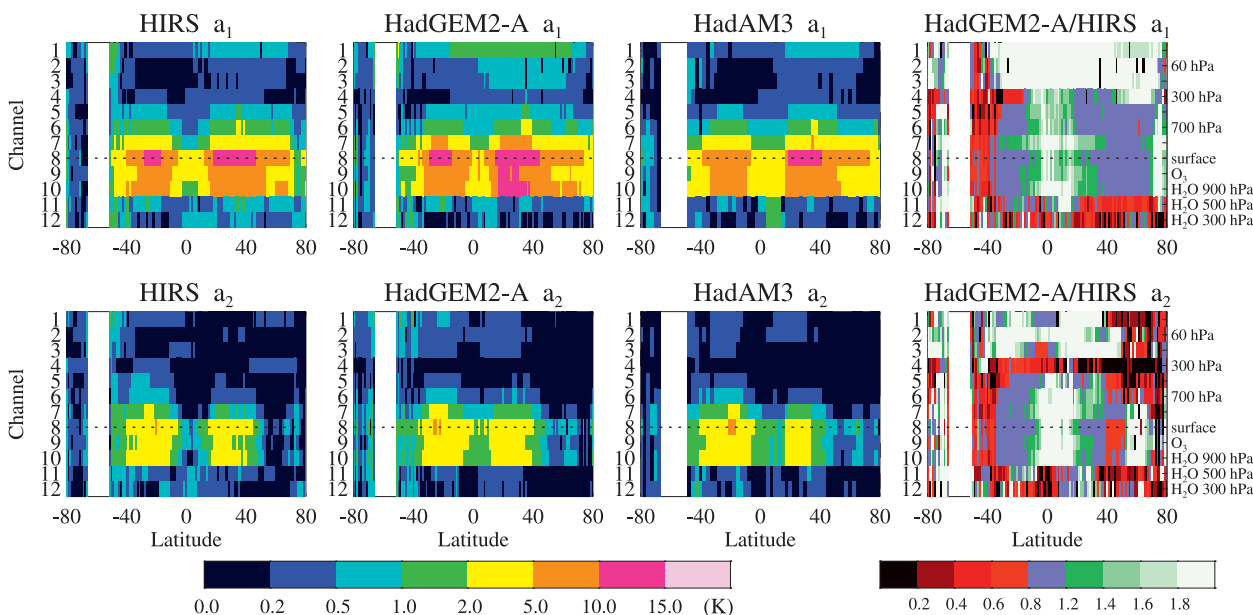
FIG. 3. Fit parameters a_1 and a_2 zonally fitted over land for July from HIRS, HadGEM2-A, and HadAM3 along with the ratio HadGEM2-A/HIRS. The labels on the secondary y axis give the sensitivity and approximate peak WF pressure of the corresponding HIRS channels. Channels 1 to 8 respond primarily to temperature changes, while chs. 9 to 12 are sensitive also to changes in atmospheric composition (see Table 1). The dotted horizontal line indicates the surface.

model samples are associated with much bigger, largely cloud-free grid boxes.

For chs. 11 and 12 (middle- and upper-tropospheric water vapor) the a_1 and a_2 amplitudes are small in both the observations and simulations, and their variation with latitude is less coherent. Nevertheless, the ratio plot reveals a general tendency for HadGEM2-A to underestimate the magnitude of the clear-sky amplitudes in these water vapor channels relative to the observations.

The seasonality of the observed and model-simulated diurnal cycles for each channel is illustrated in Fig. 4. The form of the observed seasonal cycle varies between channels, leading to a distinct seasonal pattern that is well captured by both models (top panels). In the tropospheric temperature and surface channels (4 to 8) the peak a_1 amplitudes occur during the spring and early summer as the rise in the nighttime brightness temperature minimum lags the rise in the daytime temperature maximum (shown for HIRS ch. 7). HIRS and HadGEM2-A both show a tropospheric minimum in July–August. The a_1 amplitude is smallest in winter when the maximum daily brightness temperature ($T_{b\max}$) falls further from its summertime peak than does the minimum daily temperature ($T_{b\min}$). The ozone channel 9 (which includes a sizable surface contribution) and the lower-tropospheric water vapor channel 10 behave similarly to ch. 8. Channel 11 midtropospheric water vapor behaves somewhat differently, showing a minimum a_1 amplitude in the summer and autumn

consistent with the seasonal variation in ch.-11 $T_{b\min}$ from HIRS being greater than in $T_{b\max}$ and showing a stronger summer peak (bottom, center panel).

In the upper-tropospheric water vapor channel (12) and upper-tropospheric and stratospheric temperature channels (3, 2, and 1), the evolutions of $T_{b\min}$ and $T_{b\max}$ are more in phase and although a peak monthly anomaly occurs in the temperature channels around midsummer, the seasonal variations in the anomaly are small in absolute terms compared to those at lower altitudes (see panel for HIRS ch. 1).

Equivalent plots for the Southern Hemisphere show essentially the same seasonal features both in observations and models. The overall fidelity with which both models reproduce the observations for all channels suggests that the observations are robust and that the models are successfully simulating real seasonal behavior.

Taken as a whole, the above comparisons reveal that, after accounting for the satellite sampling pattern, both of the climate models capture the major qualitative features of the HIRS observations including the form of the local diurnal cycles, their global distribution, and their seasonal variation. Figure 5 summarizes the comparison of observations and simulations in a more quantitative form showing the annual and global mean daily brightness temperature ranges (dT_br) from HIRS, HadGEM2-A, and HadAM3. These large-scale averages are statistically robust and most suitable for quantitative analysis.
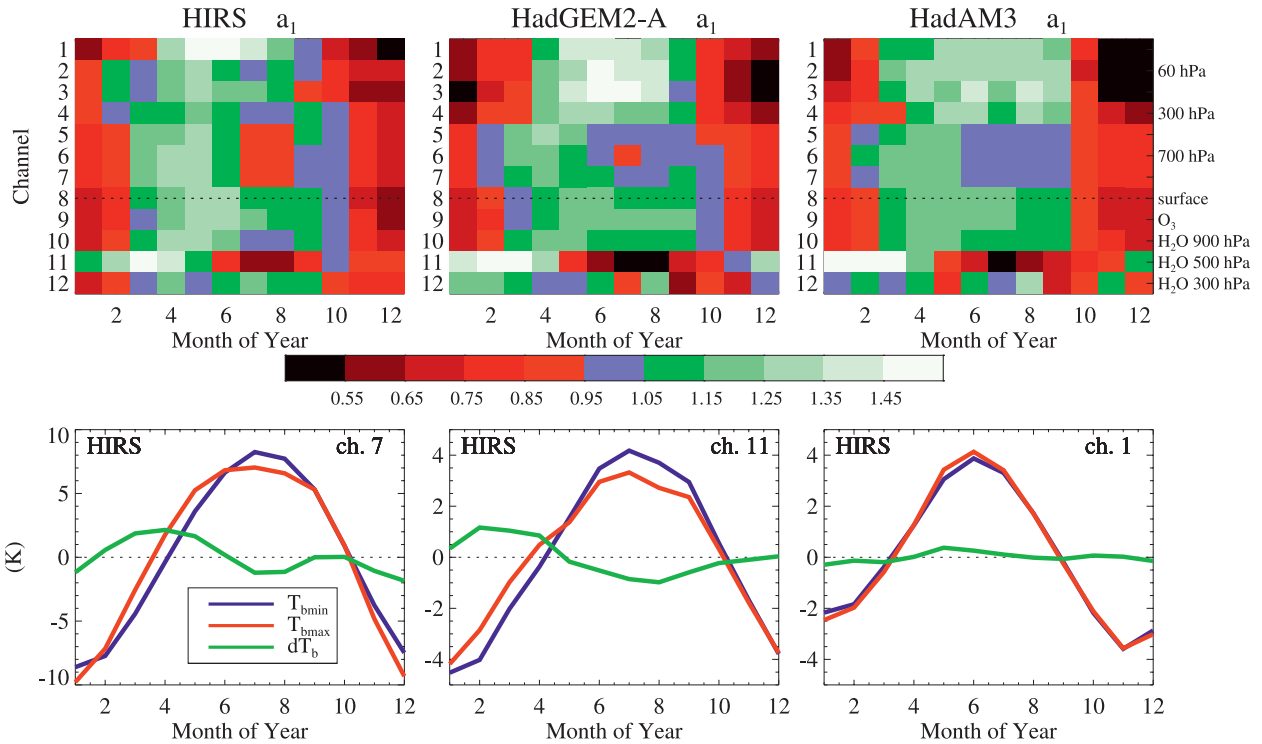
FIG. 4. (top) Monthly a_1 amplitudes for chs. 1 to 12 as a fraction of the annual mean amplitude. Results are shown from HIRS observations and HadGEM2-A and HadAM3 simulations zonally fitted over land and averaged between 20° and 60°N with area weighting. (bottom) The seasonal anomaly (monthly value minus annual mean) for the minimum and maximum brightness temperatures from the fit, T_{bmin} and T_{bmax}, and the difference, $dT_b = T_{bmax} - T_{bmin}$, for representative channels from the HIRS observations.

Over sea, the absence of any diurnal variation in the models SSTs means that the diurnal cycles simulated in the atmosphere are driven by solar forcing alone, with no surface influence. Thus, the $dT_b r$ observed over sea being systematically larger than is simulated in all the tropospheric channels 4 to 12 suggests that, in reality, variation in SST contributes significantly to the strength of the diurnal cycles observed in the troposphere, which are $O(1 \text{ K})$ in the global average. The role played by the surface in driving the tropospheric cycles is further emphasized by the much larger $dT_b r$ values seen over land than over sea in both simulations and observations. In the simulations, the difference in diurnal range over land and over sea is a direct measure of the contribution from the land surface, albeit somewhat modulated by the different global distributions of land and sea. The same holds approximately true for the observations since the measured surface (ch. 8) $dT_b r$ is an order of magnitude greater for land than for sea. Thus it can be inferred that in models and observations alike the land surface contribution dominates the solar contribution throughout the troposphere, to an extent that diminishes with altitude, in both the temperature

and water vapor channels. Models and observations concur that $dT_b r$ in chs. 1 to 3 is essentially the same over land and sea, implying that the influence of the surface is entirely lost around the tropopause and above.
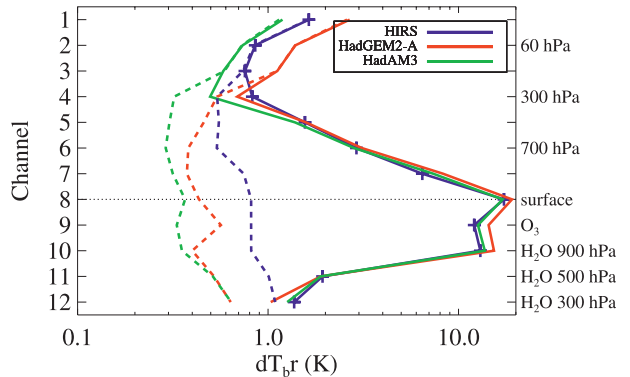

FIG. 5. Global and annual mean, daily brightness temperature ranges [$dT_b r$: difference between the maximum and minimum of the function fitted by Eq. (1)] for each HIRS channel over land (solid) and sea (dashed) from the HIRS, HadGEM2-A, and HadAM3 climatologies. Channel positions are indicated by symbols on the HIRS line. Note that the x axis has a logarithmic scale.

Over land, the agreement between simulated and observed $dT_b r$ is generally good. HadGEM2-A has a slightly stronger diurnal cycle in the channels most strongly affected by the surface than does HadAM3, which is closer to the observations. This offset in the global means is a likely consequence of the HadGEM2-A stronger diurnal cycles over desert regions noted in Fig. 2. In the midtropospheric temperature channels 5, 6, and 7 there is strong consistency between the two models and the observations, with all three showing a near-logarithmic decrease in $dT_b r$ with channel number. Although the slopes diverge somewhat in the upper troposphere between chs. 4 and 5, there is a common reversal in direction at ch. 4 with the diurnal cycle restrengthening on ascending into the stratosphere. The reversal is more pronounced in both models than in the observations.

In the stratosphere the $dT_b r$ from HIRS lies between that of the two simulations. The larger $dT_b r$ in HadGEM2-A compared to HadAM3 probably owes to a combination of the tropopause-tracking ozone scheme used in HadGEM2-A allowing the ozone profile to respond to diurnal changes in tropopause height and differences in model dynamics stemming from the finer vertical resolution of HadGEM2-A in the upper troposphere and lower stratosphere. The differences in the stratosphere notwithstanding, the suggestion from these results is that in the global, climatological sense, the climate models are successfully simulating, both qualitatively and quantitatively, the processes driving the diurnal variation observed by HIRS in the tropospheric temperature channels.

For the water vapor channels over land there is good agreement between HIRS and HadAM3 in the lower troposphere (ch. 10), whereas HadGEM2-A overestimates the diurnal temperature range probably as a result of the aforementioned overly strong diurnal cycle at the surface. In the middle troposphere, ch. 11, the $dT_b r$ values from the two models and simulations are very similar. In the upper troposphere, ch. 12, by contrast, marked differences arise between models and between models and observations; the $dT_b r$ observed by HIRS is 10% greater than that from HadAM3 and some 33% greater than that from HadGEM2-A. Given the interest in tropospheric water vapor and its role in climate-change feedback, we examine the HIRS water vapor channels and their model simulations in some more detail.

b. Mean and diurnal variability in the water vapor channels

Figure 6 shows the daily-mean brightness temperature (a_0) and the a_1 and a_2 harmonics for the water vapor channels over land from HIRS and the two models. As noted in Table 1, observed and modeled T_b in these channels depend on the water vapor distribution and on the atmospheric temperature (Soden et al. 2005), so the comparison in Fig. 6 reflects the model ability to simulate both quantities. Each model reproduces the general features of the observed daily mean brightness temperature, most notably the locations and approximate amplitudes of the subtropical maxima that are present in all three channels. These maxima coincide with regions of descent where the dryness of the air allows HIRS to see radiation emitted at higher temperatures from lower in the atmosphere. Most climate models contributing to the World Climate Research Programme (WCRP) CMIP3 archive have a moist bias in the free troposphere relative to observations (Pierce et al. 2006; John and Soden 2007), which is consistent with the chs. 11 and 12 brightness temperatures simulated from HadAM3 being lower than those measured by HIRS. HadGEM2-A, by contrast, gives generally higher T_b in these channels, suggesting an overly dry mid and upper troposphere. Despite the quantitative differences, the broad agreement between simulated and observed a_0 suggests that each model is adequately reproducing the large-scale tropospheric circulation driving the upper-tropospheric humidity distribution (Sohn et al. 2008; Chung et al. 2011).

For ch. 10 subtropical maxima occur also in the diurnal amplitudes a_1 and a_2, and again the overall form is well simulated by the both models, but with HadGEM2-A tending to more closely resemble the observations than HadAM3, particularly in the Southern Hemisphere. Both models underestimate the depth of the minima that occur in the tropical wet convecting region for all three ch. 10 fit parameters. This may be related to the aforementioned sampling biases arising between HIRS and the climate models in regions of prevalent convective cloud.

In the middle and upper troposphere (chs. 11 and 12) the observed latitudinal dependence of the diurnal amplitudes a_1 and a_2 is quite different from that of the mean values a_0. The amplitudes at these altitudes are small and consequently partially obscured by weather noise, but nevertheless the models produce amplitudes of magnitude comparable to the observations and showing somewhat similar variation with latitude, although there are considerable differences of detail. The spike in the a_1 amplitudes around ~40°N stems from a strong peak over the Himalayan plateau, and is underestimated by the models because the underlying orography is not fully resolved. Similarly, the peak observed at ~40°S occurs where the few measurements over land are dominated by the Andes, which are barely resolved in the models. The tropical and subtropical a_1 amplitudes
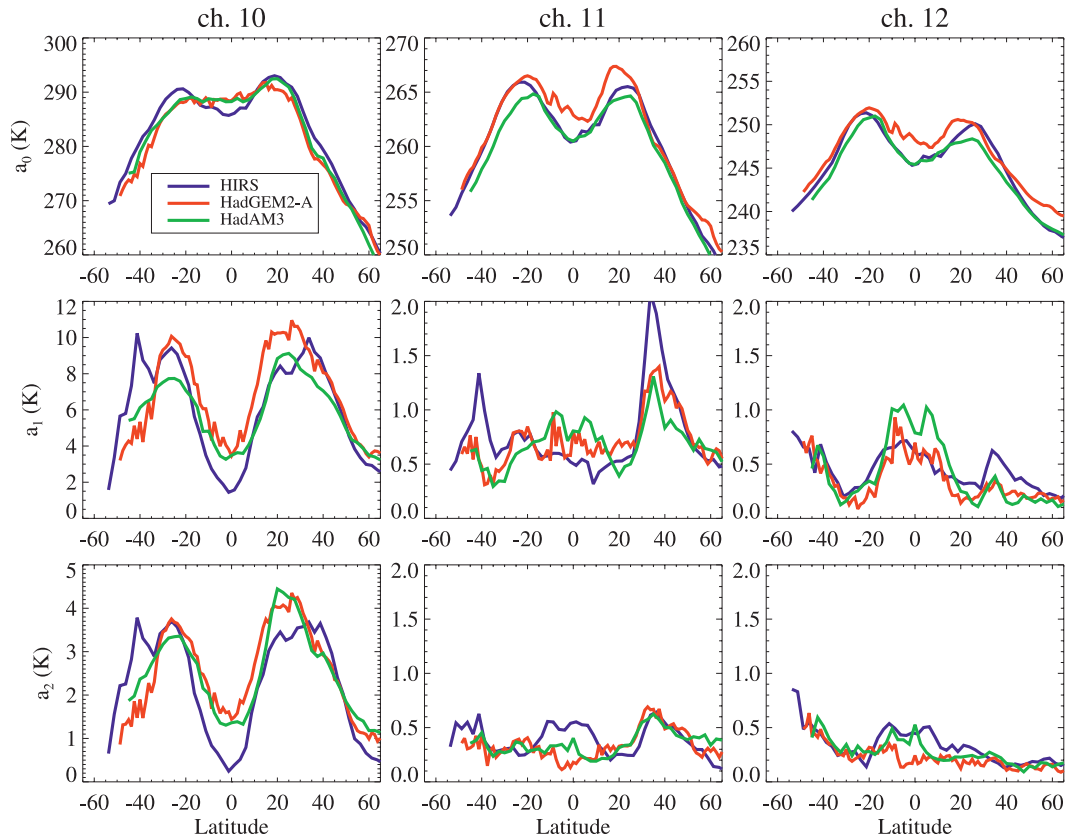
FIG. 6. The annual mean of the a_0, a_1, and a_2 Fourier fit parameters [Eq. (1)] for water vapor channels 10, 11, and 12 zonally fitted over land from HIRS, HadGEM2-A, and HadAM3 climatologies. The latitudinal resolution is 2.5° for HIRS and HadAM3 and 1.25° for HadGEM2-A. Note that the scale of the y axis changes between panels.

are overestimated by both models for ch. 11, and by HadAM3 for ch. 12, where HadGEM2-A is closer to the observations. Conversely, both models generally underestimate the a_2 amplitudes in both channels, especially in the low latitudes where HadGEM2-A entirely misses the observed tropical maximum while HadAM3 fails to reproduce its magnitude and meridional extent. The daily T_b ranges shown in Fig. 5 are a phase-dependent summation of the a_1 and a_2 amplitudes shown here; although the $dT_b r$ in chs. 11 and 12 from HadAM3 are close to those observed, these results imply that there are compensating errors in the relative contributions of the a_1 and a_2 components. These errors have implications for the inference of diurnal sampling biases in the HIRS record (section 5).

Overall, the results suggest that the climate models are capturing the major processes controlling the magnitude and variability of the daily-mean, clear-sky brightness temperatures measured in all the HIRS water vapor channels, and for ch. 10 also the magnitude and variability of the diurnal and semidiurnal amplitudes. However, for chs. 11 and 12, although the simulations and observations agree that the a_1 and a_2 amplitudes

are relatively small, the intermodel differences and the failure of either model to reproduce either qualitatively or quantitatively the full detail of the observed daily cycle suggest a general model shortcoming in the representation of the diurnal behavior of the middle- and upper-tropospheric water vapor channels.

The weak diurnal cycles found here for chs. 11 and 12 are qualitatively consistent with the climate model-based diurnal corrections of Jackson and Soden (2007), which have been applied to HIRS data used to study upper-tropospheric humidity (Chung et al. 2011). However, the failure of both climate models, HadGEM2-A and HadAM3, to capture the detailed form of the diurnal cycle urges the need for careful validation of climate model performance prior to using model-adjusted brightness temperature measurements to derive small climate trends in atmospheric water vapor.

c. Phase of the diurnal cycle

In addition to the amplitude, the phase of the simulated diurnal cycle is another important measure of model performance. We examine the phase using t_{max},
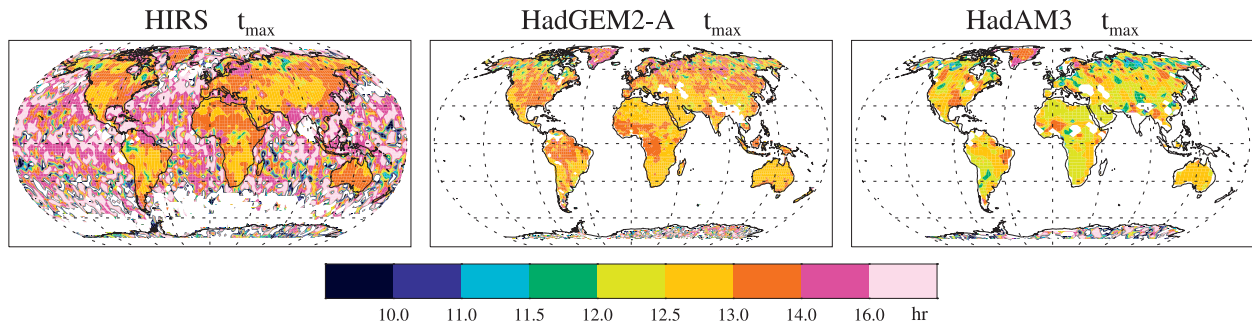
FIG. 7. The local time of maximum ch. 8 brightness temperature, t_{max}, for July from HIRS observations and HadGEM2-A and HadAM3 simulations. Simulated results over ocean are omitted (see text).

the local time of maximum brightness temperature, which combines the phases of the 24- and 12-hourly oscillations t_1 and t_2 as defined in Eq. (1). Usually t_{max} is close to t_1. Figure 7 shows maps of t_{max} for ch. 8 and July from HIRS, HadGEM2-A, and HadAM3. In observations and both models the phase is fairly uniform and coherent over land with t_{max} in the early afternoon. The observed t_{max}, usually between 1250 and 1400 local time, is fairly well matched by HadGEM2-A although it tends to be a little earlier in the model, particularly over northern Africa (as seen also in Fig. 1) and Australia. HadAM3, however, has a more pronounced early bias in t_{max} compared with the observations, with peak T_b occurring between 12 and 12.5 over large areas of Africa, Europe, and South America. The phases from HIRS and HadGEM2-A are largely consistent with, though sometimes slightly earlier than, the Cloud Archive User Service (CLAUS) compilation of window-channel satellite measurements, which shows peak T_b occurring 1 to 2 h after local noon over clear-sky tropical land areas (Yang and Slingo 2001). The summer diurnal cycle of 2-m temperature over Kansas grassland is also found to peak 1–2 h after noon (Betts and Ball 1995).

The HIRS-observed t_{max} over sea is less coherent than over land and tends to lag the land values, with peak T_b most commonly occurring between 1400 and 1600 local time, in agreement with the CLAUS data that shows peak T_b occurring in mid to late afternoon over clear-sky tropical ocean. Owing to the lack of diurnal cycle in model SST, the t_{max} simulated over sea is dominated by noise and is not shown.

The phases over land from the zonally fitted data for July are shown for all channels in Fig. 8. Observations and simulations give qualitatively similar distributions; t_{max} is in early afternoon for chs. 5 to 10 and late afternoon or early evening for the mid- and upper-tropospheric water vapor and stratospheric channels. Jackson and Soden (2007) in their HIRS simulations also find t_{max} to be later in the upper-tropospheric water vapor channels

than in the channels sensitive to the surface and lower stratosphere. Diurnal temperature phases later than 1600 local time are reported in radio occultation data from the tropical upper troposphere and lower stratosphere (Zeng et al. 2008).

The zonal distributions from HIRS, HadGEM2-A, and HadAM3 are all similar, most markedly for chs. 5 to 7 where t_{max} is latest in the tropics and the higher northern latitudes. Quantitatively, the difference plot confirms that for the surface and bulk of the troposphere (chs. 5 to 10) the t_{max} from HadGEM2-A is within 30 min of the observations, with a larger difference occurring in the tropics where the simulated t_{max} is earlier than observed. The t_{max} simulated by HadGEM2-A for the upper troposphere and stratosphere (chs. 1 to 3), which will be strongly influenced by shortwave heating, is generally some 2 h later than is observed except for the high northern latitudes where the observed t_{max} is later and lags the simulations. As with the a_2 amplitudes, the simulated ch.-4 phases are notably different from the observations, having a later t_{max}. For the most part the HadGEM2-A t_{max} for midtropospheric water vapor channel 11 is earlier than observed whereas for the upper-tropospheric water vapor, ch. 12, the HadGEM2-A t_{max} tends to be later. These phase differences are another indicator of possible model deficiencies in the water vapor channels.

Notwithstanding the earlier t_{max} from HadAM3 for the near-surface channels, the overall phase distributions from the two models are closer to each other than either model is to the observations. This suggests that the phase of the simulated diurnal cycle is controlled by large-scale processes common to both models that are not fully matching the observed atmosphere.

4. Sensitivity to model sampling pattern

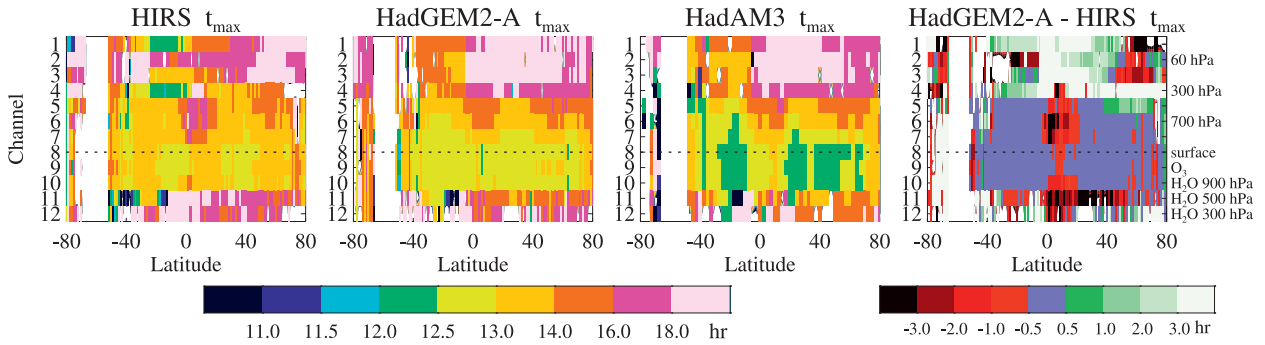Having examined how diurnal cycles in brightness temperature derived from HIRS-like sampling of two

FIG. 8. The local time of maximum brightness temperature, t_{max}, in chs. 1 to 12 for HIRS observations and HadGEM2-A and HadAM3 simulations zonally fitted over land for July, along with the difference HadGEM2-A minus HIRS.

climate models compare to the diurnal cycles derived from the HIRS observations themselves, we now question how the satellite sampling impacts the form of the fitted cycles. We do this by preparing a further simulated diurnal climatology, exploiting the full hourly frequency of model data available at every grid box instead of merely that subset of the grid box data included in the HIRS-like sampling. To this end, brightness temperatures were calculated for every HadGEM2-A grid box with cloud fraction less than 0.4 in each hourly, global HadGEM2-A output. Over the six years of integration this gives a good sampling of the brightness temperatures at every hour of the day over virtually the whole globe. The brightness temperatures from this full hourly model sampling were then Fourier fitted as before to generate, for each grid box and month, a "true" model diurnal cycle against which the cycle derived from the more limited HIRS-like, along-track sampling could be evaluated.

Figure 9 compares the HIRS-sampled and fully sampled Fourier fits from HadGEM2-A for the same channels and grid boxes as shown in Fig. 1. The figure emphasizes the excellent daily temporal coverage provided by the four satellites operating between 2002 and 2007 and their orbital drift, with at least one simulated HIRS sample being taken from almost every model hour over the period of integration. However, because there are fewer simulations at each hour from the HIRS-like sampling than from the full sampling, the natural variability is less well captured. (For a more cloudy grid box both samplings will be more sparse.) In ch. 8, where the amplitude of the diurnal cycle is large relative to the natural variability at each local time, the fully sampled and HIRS-sampled fits are in close agreement and a_1 and a_2 are little changed. For ch. 5 the amplitude of the diurnal cycle is smaller relative to the natural variability, so the reduced sampling of each hour causes a more marked divergence of the HIRS-sampled fit from the true diurnal behavior and exaggerates the importance of the semidiurnal variation a_2 relative to a_1.

Figure 9 also shows the fits obtained by using the fully sampled data at reduced frequencies of 3- and 6-hourly as opposed to 1-hourly. Here we are retaining the full variability at each of the sampling times but decreasing
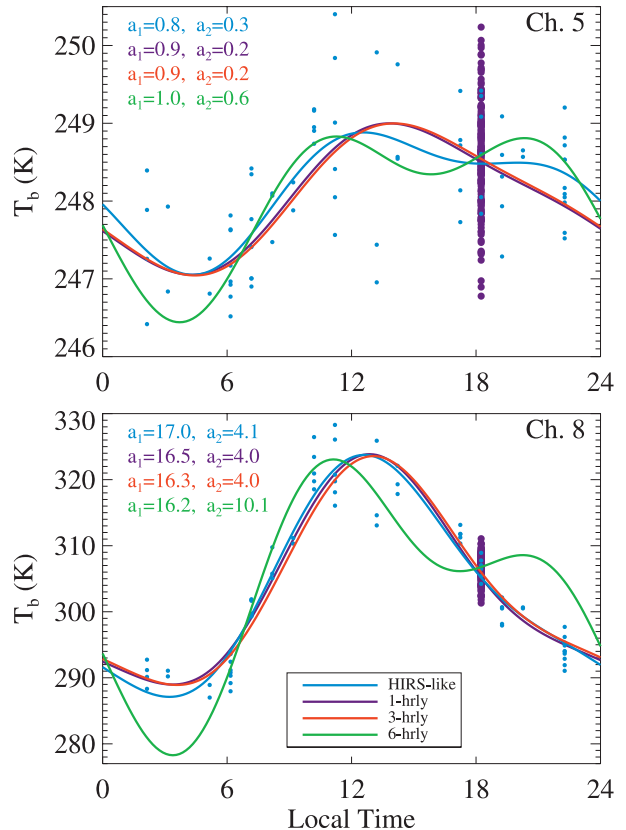
FIG. 9. Fourier fits to clear-sky brightness temperatures simulated from HadGEM2-A for the same channels, grid box, month, and integration period as Fig. 1. Fits are shown for 1-, 3-, and 6-hourly sampling of the model grid box along with the grid box sampled as seen by HIRS. Individual points are shown for the HIRS-like sampling and for the full model sampling at ~1800 local time. Individual points from other hours of the full sampling are omitted for clarity.
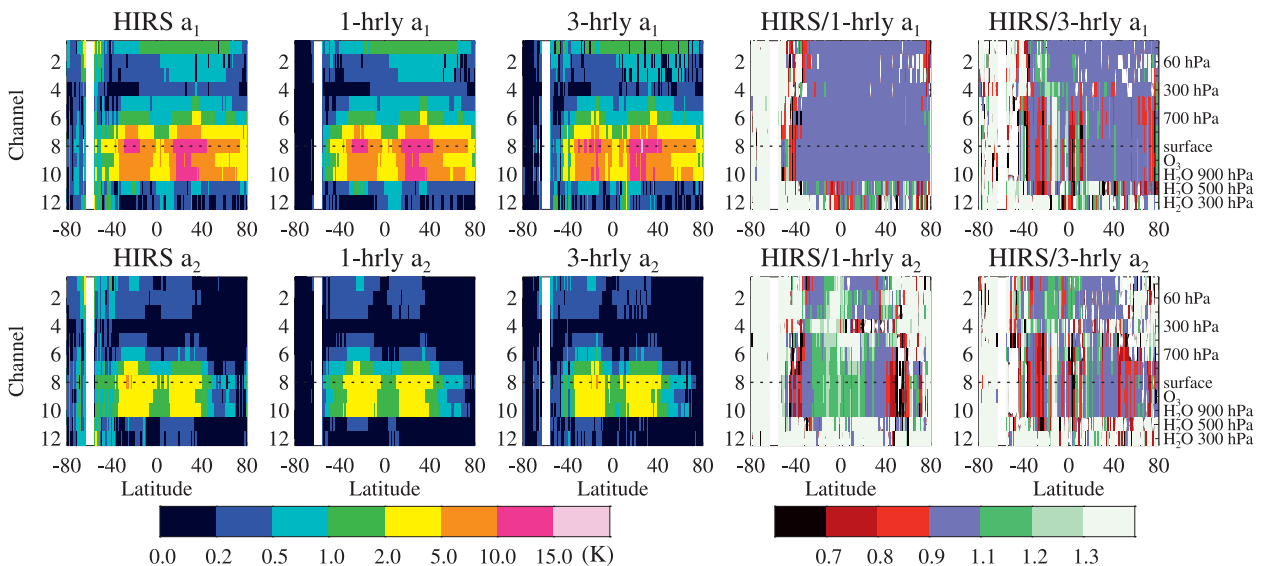
FIG. 10. Fourier fit parameters a_1 and a_2 zonally fitted over land for July from HIRS-like and 1- and 3-hourly sampling of every clear-sky HadGEM2-A grid box. The panels on the right show the values as a fraction of the 1-hourly sampled values.

the number of sampling times. Reducing the sampling frequency to 3-hourly causes only a slight degradation in the diurnal fit for both channels through reducing the curvature and marginally shifting the timing of the peak in ch. 8. With 6-hourly sampling the diurnal cycle is poorly constrained and spurious a_2 amplitudes are introduced in both channels, resulting in clearly unrealistic fits.

The global impact of the different sampling strategies on the diurnal and semidiurnal amplitudes calculated from the HadGEM2-A simulations is shown in Fig. 10, disregarding the poor 6-hourly results. The general distributions of the two amplitudes change little with the different sampling methods. Aside from the noisy and poorly sampled high southern latitudes, the ratio plots indicate that the largest fractional differences occur in the water vapor channels 11 and 12 where the amplitudes are small and disproportionately affected by weather noise. The fractional differences are generally greater for a_2 than for a_1 because the a_2 absolute amplitudes are smaller. Reducing the sampling tends to bias the amplitudes high as the fit becomes less constrained.

It is notable that, particularly for a_1, the HIRS-like sampling more closely resembles the 1-hourly sampling than does the 3-hourly sampling; this underlines the comprehensive coverage of the full diurnal cycle available from the HIRS observations during the period chosen for analysis. Moreover, the similarity of the amplitudes inferred from the HIRS-like and the fully (i.e., 1 hourly) sampled model supports the methodology used by Lindfors et al. (2011) to develop

their diurnal climatology of brightness temperatures from HIRS observations. The reduced sampling of the natural variability by the HIRS instruments is less important in these zonally fitted results than for the single model grid box shown in Fig. 9. Also, differences in the natural variability in the atmosphere versus the internal variability of the model, and the different spatial scales of the HIRS measurements and the model grid boxes, may somewhat modulate the sensitivity to the sampling employed. Nevertheless these model results lend confidence that the Lindfors et al. climatology is representative of true atmospheric behavior and largely free from bias introduced by the satellites' measurement pattern.

The general similarity of the zonal diurnal fits obtained from regular sampling of the climate model at 1- and 3-hourly frequencies seen in Fig. 10 suggests that, for many studies of diurnal cycles in simulated brightness temperatures, retaining 3-hourly model output will be sufficient to capture the salient features of the model behavior. On the other hand, the differences of detail between the HIRS-like and regular samplings of the model (Figs. 9 and 10) imply that fully quantitative model-measurement comparison does require that the along-track satellite viewing pattern be emulated with the model.

5. Diurnal temperature biases

One motivation for characterizing the observed and simulated diurnal cycles in brightness temperatures is to enable accounting for diurnal biases in the HIRS record

when comparing measured and modeled decadal trends. Here we examine how the observed and simulated diurnal cycles combined with the orbit characteristics of the NOAA satellites translate into brightness temperature biases in the HIRS record. The *NOAA-14* satellite, which was long lived and had a large orbital drift during its period of operation (Lee et al. 2007), is used as an example. Because *NOAA-14*, in common with all the HIRS satellites, is in a sun-synchronous orbit, it measures each latitude at two local times per day, once in the ascending orbit mode and once in the descending. For a stable orbit these times are fixed, but with orbital drift the local times change over the duration of the mission, introducing a diurnal bias into the measurement record.

For any given latitude, month, and local time a brightness temperature can be obtained from Eq. (1) using the derived climatologies of diurnal fit parameters. Brightness temperatures were calculated in this way for each month of the *NOAA-14* era from 1995 to 2007 using diurnal parameters zonally fitted over land from both the HIRS and the HadGEM2-A (with HIRS-like sampling) climatologies. The brightness temperature calculated for any given month and latitude varies with year owing to the change in local times at which the *NOAA-14* measurements were made. The monthly results were then averaged, including all ascending and descending mode measurements, to obtain an annual-mean brightness temperature for each year of *NOAA-14* operation. Figure 11 shows, as a function of latitude, the difference between the largest and the smallest annual-mean ch. 8 brightness temperatures obtained for the *NOAA-14* era. These interannual differences stem entirely from the diurnal variation of T_b coupled with the drifting local time of the HIRS measurements. Brightness temperatures differences (biases) arising from the a_1 and a_2 components of the diurnal cycles are shown separately.

As expected given the consistency of the observed and simulated fit parameters, the diurnal brightness temperature biases derived from the HIRS and HadGEM2-A climatologies are generally similar, both in distribution and in magnitude. The finer resolution of HadGEM2-A compared to the gridded HIRS data introduces some extra structure in the model results and slightly displaces the simulated and observed distributions. HadGEM2-A underestimates the fitted amplitudes and hence the biases between 40° and 50°S because the orography over the tip of South America, the only landmass at these latitudes, is underresolved in the model.

In the tropical latitudes the ascending and descending measurements are taken close to 12 h apart, so the a_1 (24 hourly) component of the diurnal variation averages out and the corresponding temperature differences are close to zero. The a_1 contribution to the difference in
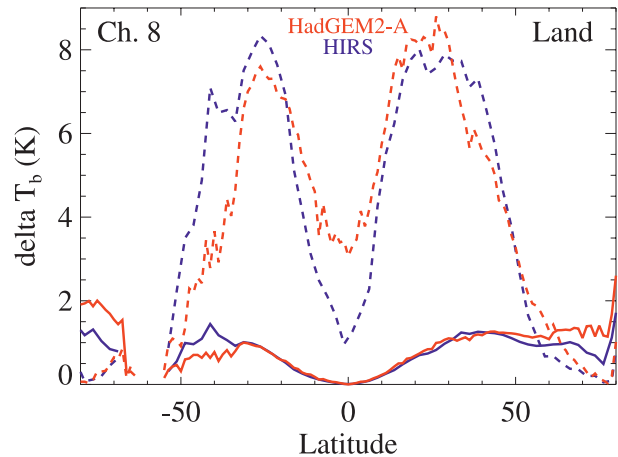

FIG. 11. The difference between the largest and smallest annual-mean ch.-8 T_b calculated for the *NOAA-14* operating period. The T_b were obtained from Eq. (1) using a_{1-2} and t_{1-2} parameters zonally fitted over land from the HIRS and HadGEM2-A (HIRS-like sampling) diurnal climatologies along with the local times of the *NOAA-14* measurements for each month. See text for further explanation. The T_b differences due to the a_1 and a_2 components of the diurnal cycle are shown separately as solid and dashed lines respectively. The latitudinal resolution is 2.5° for HIRS and 1.25° for HadGEM2-A.

brightness temperature grows with latitude as the local time difference between ascending and descending measurements decreases from 12 h. Nevertheless, at all low and middle latitudes the temperature bias is dominated by the a_2 component, which is responsible for brightness temperature differences of up to ~8 K in the Northern and Southern Hemisphere subtropics where there is a high contribution from dry desert regions with a large diurnal variation in land surface temperature.

Whereas the observations imply that the a_2 temperature bias at the equator falls to ~1 K, the simulations, although also showing an equatorial minimum, have the a_2 bias remaining above 3 K. This is consistent with the HadGEM2-A overestimate of the tropical amplitudes in the near-surface channels noted in Fig. 4. Similarly, the model overestimate of the a_1 bias at the highest latitudes follows from the larger HadGEM2-A amplitudes over northern Canada, Greenland, and Antarctica evident in Fig. 2. Although the associated phases t_1 and t_2 also influence the inferred biases, the differences in the T_b biases inferred from HIRS and from HadGEM2-A are dominated by the differences in the a_1 and a_2 amplitudes themselves.

The biases for other channels over land follow a similar latitudinal distribution to those shown here for ch. 8, while over sea the distributions are flatter and the biases of smaller magnitude. The results are summarized in Fig. 12, which shows the T_b biases for all HIRS channels
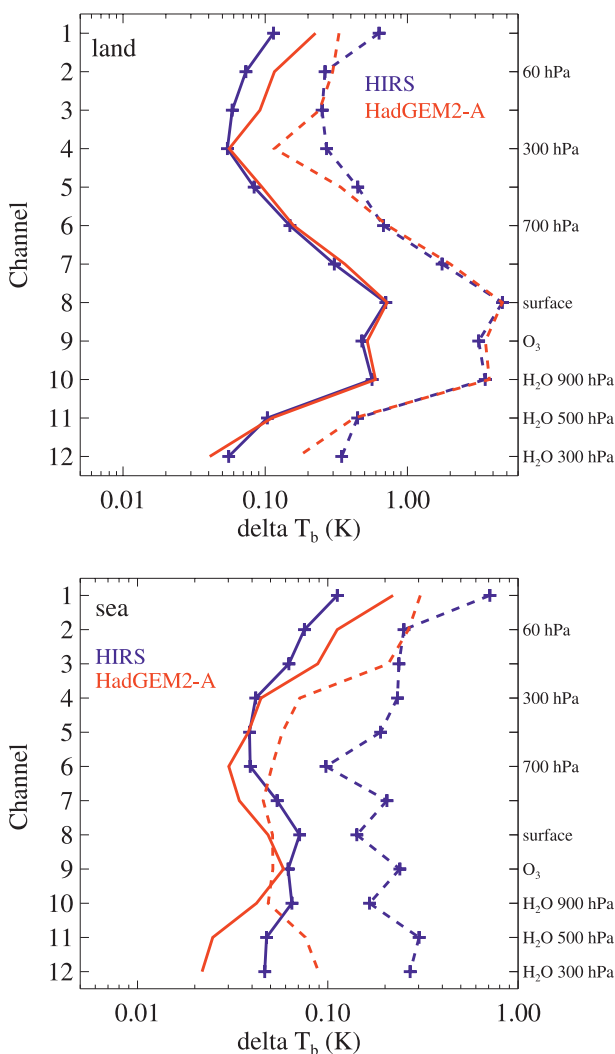
FIG. 12. The global mean of the annual mean T_b differences shown in Fig. 11 for each HIRS channel and for Fourier parameters zonally fitted separately over land and sea. The a_1 and a_2 contributions are shown as solid and dashed lines respectively. Note that the x axis has a logarithmic scale.

over both land and sea as a global mean. Over land, the biases observed and simulated for most channels are highly quantitatively consistent both for the a_1 and a_2 contributions. The dominance of the a_2 component over a_1 is emphasized in the area-weighted global mean because of the small a_1 values around the equator. Maximum temperature biases of 4–5 K occur in the strongly surface-influenced channels 8, 9, and 10 and diminish with height through the midtropospheric temperature channels 5, 6, and 7, with similar slope in observations and simulations and in the a_1 and a_2 components. Some discrepancy arises in the upper-tropospheric and stratospheric channels 1–4, where HadGEM2-A shows a sharper reversal of gradient than does HIRS.

A marked discrepancy also occurs in the upper-tropospheric water vapor channel 12 over land where the a_2 bias implied by the HIRS diurnal climatology exceeds that implied by the HadGEM2-A climatology by more than 50%. This fractional difference in the T_b bias is markedly larger than that in the diurnal T_b range seen in Fig. 5 because, as shown in Fig. 6, HadGEM2-A underestimates the a_2 amplitude relative to HIRS while getting the a_1 amplitude approximately correct. This result emphasizes that accurate simulation of diurnal temperature biases requires capturing not merely the daily range, but also the detailed form of the diurnal cycle in brightness temperature. The close agreement for ch. 11 in the global mean masks differences in the latitudinal distributions of the observed and simulated amplitudes for this channel.

Over sea, consistent with the lack of diurnal variation in model SST, the simulated tropospheric biases are smaller than their observed counterparts, and all except the observed a_2 are below 0.1 K. That the observed a_2 biases are markedly larger than those simulated with HadGEM2-A suggests that they are a robust consequence of a real diurnal variation in T_b driven by the daily cycle in SST. Although the T_b biases observed over sea are an order of magnitude smaller than those observed over land, they are of similar size to the expected climate trend of 0.1 to 0.2 K over the 12 years of *NOAA-14* operation. Thus, even when considering measurements over sea only, diurnal sampling effects should be accounted for in deriving climate signals from HIRS observations.

The overall indications from these comparisons are that when HadGEM2-A is sampled according to the HIRS viewing pattern, the global-mean diurnal T_b biases occurring in the tropospheric temperature channels over land closely parallel those in the HIRS observational record. However, larger fractional errors can occur in the upper-tropospheric water vapor channel due to incorrect partitioning of the diurnal cycle between the 24- and 12-hourly (a_1 and a_2) components.

6. Conclusions

Clear-sky brightness temperature measurements from the High-Resolution Infrared Radiation Sounder (HIRS) were simulated with two Hadley Centre climate models, HadGEM2-A and HadAM3, via the RTTOV radiative transfer package. By sampling the model atmospheres according to the HIRS viewing pattern, climatologies of model-simulated diurnal cycles in HIRS brightness temperatures were developed analogous to the observationally based climatology of Lindfors et al. (2011). Comparison of the climatologies enables an evaluation of model performance in reproducing the observed diurnal behavior, which in turn is a test of the underlying

model physics and representation of key atmospheric processes.

Over land, there is good agreement between simulations and observations for most HIRS measurement channels, both in the mean strength and phase of the diurnal cycles and in their spatial and seasonal variation. The consistency between models and the observations is especially high for the tropospheric temperature channels, where the amplitudes of the diurnal variations on ascending from the surface to the upper troposphere decrease with near-uniform slopes. The strength of the agreement is perhaps surprising given that free-tropospheric diurnal temperature variation is not a quantity typically monitored during model development. An intermodel bias in the near surface channels is most likely a product of the different surface exchange schemes used. Maximum brightness temperatures in the surface and lower- to middle-tropospheric channels occur between 1250 and 1400 local time in the HIRS observations, compared with the 1300 to 1400 range commonly found in previous measurements. The time of temperature maximum simulated from HadGEM2-A is slightly earlier than seen by HIRS while HadAM3 shows a more pronounced early bias relative to the observations.

The models agree with the observations and with previous model studies that clear-sky diurnal cycles in the middle- and upper-tropospheric water vapor channels are relatively weak, with amplitudes $O(0.5\ K)$. However, the annual, global means of the simulated diurnal brightness temperature ranges in those water vapor channels are up to a third smaller than are observed, and there are differences of phase. There are also notable intermodel differences. The low resolution of cloudy and cloud-free regions in the climate models relative to the HIRS measurements limits the use of clear-sky data to assess model simulations of water vapor in the actively convecting tropics where the net diurnal cycle in upper-tropospheric humidity is strongly tied to the diurnal cycle in convection (e.g., Soden 2000; Tian et al. 2004).

Over sea, the lack of any diurnal variability in the model prescribed SSTs causes the models to underestimate the diurnal cycles (which are themselves small) measured from the surface up to the upper troposphere in both temperature and water vapor channels. Models and observations agree that the diurnal cycles over land are strongly influenced by the surface throughout most of the troposphere but become independent of the surface from around the tropopause upward where the cycles have equal amplitude over land and sea. Maximum brightness temperatures near the sea surface in the HIRS observations typically occur at least two hours later than over land, consistent with other satellite measurements.

For most channels over land, diurnal sampling biases associated with drift in the local times of HIRS measurements are similar when inferred from the observed and simulated climatologies. The biases observed over sea, missed by the simulations, are much smaller than over land but are still comparable in magnitude with the expected climate trend in tropospheric temperature. In the global mean, biases for all channels are dominated by the 12-hourly harmonic of the diurnal cycle. For the upper-tropospheric water vapor channel over land, differences between simulations and observations in the relative contributions of the 24- and 12-hourly harmonics to the diurnal cycle lead to large fractional differences in the inferred sampling bias.

Climatological diurnal cycles derived from the fully sampled model (every clear-sky grid point, every hour) differ little from those derived from the HIRS-like sampled model. This implies that the HIRS measurements are sufficient to constrain the full form of the actual atmospheric cycles and, thus that the Lindfors et al. (2011) observationally based climatology is representative of real atmospheric behavior.

In total, these results establish that, in the global mean, the current and recent generation of atmospheric models, as represented here by Hadley Centre models HadGEM2-A and HadAM3, well reproduce the radiative, physical, and dynamical processes driving the diurnal cycles in clear-sky brightness temperature. This, in turn, may suggest that the diurnal cycles themselves are essentially large-scale phenomena relatively insensitive to details of model formulation and parameterization. In addition to constituting a general validation of model-simulated diurnal cycles, the results support the use of climate models in correcting diurnal sampling biases in long-term records of atmospheric brightness temperatures as measured by HIRS and other satellite instruments such as the Microwave Sounding Unit. However, it is also demonstrated that, particularly in the water vapor channels, careful validation is required to ensure that the applied model captures not only the gross features, but also the fine detail of the real diurnal behavior. Nonetheless, the general consistency of the observed and simulated diurnal biases hints at the possibility of meaningfully comparing small climate trends in brightness temperatures extracted from observations and from model simulations, both as a test of climate model performance and to help elucidate key atmospheric processes such as the role of water vapor feedback.

REFERENCES

Allan, R. P., M. A. Ringer, and A. Slingo, 2003: Evaluation of moisture in the Hadley Centre climate model using simulations of HIRS water-vapour channel radiances. *Quart. J. Roy. Meteor. Soc.,* **129,** 3371–3389, doi:10.1256/qj.02.217.

Bates, J. J., and D. L. Jackson, 2001: Trends in upper-tropospheric humidity. *Geophys. Res. Lett.,* **28,** 1695–1698.

Betts, A., and J. Ball, 1995: The FIFE surface diurnal cycle climate. *J. Geophys. Res.,* **100** (D12), 25 679–25 693.

Bodas-Salcedo, A., and Coauthors, 2011: COSP: Satellite simulation software for model assessment. *Bull. Amer. Meteor. Soc.,* **92,** 1023–1043.

Chung, E.-S., and B. J. Soden, 2010a: Investigating the influence of carbon dioxide and the stratosphere on the long-term tropospheric temperature monitoring from HIRS. *J. Appl. Meteor. Climatol.,* **49,** 1927–1937.

——, and ——, 2010b: Radiative signature of increasing atmospheric carbon dioxide in HIRS satellite observations. *Geophys. Res. Lett.,* **37,** L07707, doi:10.1029/2010GL042698.

——, ——, B.-J. Sohn, and J. Schmetz, 2011: Model-simulated humidity bias in the upper troposphere and its relation to the large-scale circulation. *J. Geophys. Res.,* **116,** D10110, doi:10.1029/2011JD015609.

Collins, W. J., and Coauthors, 2008: Evaluation of the HadGEM2 model. Hadley Centre Tech. Note HCTN 74, 47 pp. [Available online at http://www.metoffice.gov.uk/archive/science/climate-science/hctn74.]

——, and Coauthors, 2011: Development and evaluation of an Earth-system model—HadGEM2. *Geosci. Model Dev.,* **4,** 1051–1075, doi:10.5194/gmd-4-1051-2011.

Cox, P. M., R. A. Betts, C. B. Bunton, R. L. H. Essery, P. R. Rowntree, and J. Smith, 1999: The impact of new land surface physics on the GCM simulation of climate and climate sensitivity. *Climate Dyn.,* **15,** 183–203.

Engelen, R., L. Fowler, P. Gleckler, and M. Wehner, 2000: Sampling strategies for the comparison of climate model calculated and satellite observed brightness temperatures. *J. Geophys. Res.,* **105** (D7), 9393–9406.

Essery, R. L. H., M. J. Best, R. A. Best, P. M. Cox, and C. M. Taylor, 2003: Explicit representation of subgrid heterogeneity in a GCM land surface scheme. *J. Hydrometeor.,* **4,** 530–543.

Gettelman, A., and Q. Fu, 2008: Observed and simulated upper-tropospheric water vapor feedback. *J. Climate,* **21,** 3282–3289.

Held, I., and B. Soden, 2000: Water vapor feedback and global warming. *Annu. Rev. Energy Environ.,* **25,** 441–475, doi:10.1146/annurev.energy.25.1.441.

Iacono, M. J., J. S. Delamere, J. S. Mlawer, and S. A. Clough, 2003: Evaluation of upper tropospheric water vapor in the NCAR Community Climate Model (CCM3) using modeled and observed HIRS radiances. *J. Geophys. Res.,* **108,** 4037, doi:10.1029/2002JD002539.

Jackson, D. L., and B. J. Soden, 2007: Detection and correction of diurnal sampling bias in HIRS/2 brightness temperatures. *J. Atmos. Oceanic Technol.,* **24,** 1425–1438.

John, V. O., and B. J. Soden, 2007: Temperature and humidity biases in global climate models and their impact on climate feedbacks. *Geophys. Res. Lett.,* **34,** L18704, doi:10.1029/2007GL030429.

——, G. Holl, R. P. Allan, S. A. Buehler, D. E. Parker, and B. J. Soden, 2011: Clear-sky biases in satellite infrared estimates of upper tropospheric humidity and its trends. *J. Geophys. Res.,* **116,** D14108, doi:10.1029/2010JD015355.

Johns, T., and Coauthors, 2006: The new Hadley Centre Climate Model (HadGEM1): Evaluation of coupled simulations. *J. Climate,* **19,** 1327–1353.

Jones, C. D., and Coauthors, 2011: The HadGEM2-ES implementation of CMIP5 centennial simulations. *Geosci. Model Dev.,* **4,** 543–570, doi:10.5194/gmd-4-543-2011.

Lee, H.-T., A. Gruber, R. G. Ellingson, and I. Laszlo, 2007: Development of the HIRS outgoing longwave radiation climate dataset. *J. Atmos. Oceanic Technol.,* **24,** 2029–2047.

Li, J., W. W. Wolf, W. P. Menzel, W. Zhang, H.-L. Huang, and T. H. Achtor, 2000: Global soundings of the atmosphere from ATOVS measurements: The algorithm and validation. *J. Appl. Meteor.,* **39,** 1248–1268.

Lindfors, A. V., I. A. MacKenzie, S. F. B. Tett, and L. Shi, 2011: Climatological diurnal cycles in clear-sky brightness temperatures from the high-resolution infrared radiation sounder (HIRS). *J. Atmos. Oceanic Technol.,* **28,** 1199–1205.

Martin, G. M., M. A. Ringer, V. D. Pope, A. Jones, C. Dearden, and T. J. Hinton, 2006: The physical properties of the atmosphere in the new Hadley Centre Global Environmental Model (HadGEM1). Part I: Model description and global climatology. *J. Climate,* **19,** 1274–1301.

Matricardi, M., 2009: Technical note: An assessment of the accuracy of the RTTOV fast radiative transfer model using IASI data. *Atmos. Chem. Phys.,* **9,** 6899–6913.

——, F. Chevallier, G. Kelly, and J. Thépaut, 2004: An improved general fast radiative transfer model for the assimilation of radiance observations. *Quart. J. Roy. Meteor. Soc.,* **130,** 153–173, doi:10.1256/qj.02.181.

Mears, C., and F. Wentz, 2005: The effect of diurnal correction on satellite-derived lower tropospheric temperature. *Science,* **309,** 1548–1551, doi:10.1126/science.1114772.

——, M. Schabel, and F. Wentz, 2003: A reanalysis of the MSU channel 2 tropospheric temperature record. *J. Climate,* **16,** 3650–3664.

Pierce, D., T. Barnett, E. Fetzer, and P. Gleckler, 2006: Three-dimensional tropospheric water vapor in coupled climate models compared with observations from the AIRS satellite system. *Geophys. Res. Lett.,* **33,** L21701, doi:10.1029/2006GL027060.

Pope, V. D., M. L. Gallani, P. R. Rowntree, and R. A. Stratton, 2000: The impact of new physical parametrizations in the Hadley Centre climate model: HadAM3. *Climate Dyn.,* **16,** 123–146, doi:10.1007/s003820050009.

Rayner, N. A., D. E. Parker, E. B. Horton, C. K. Folland, L. V. Alexander, D. P. Rowell, E. C. Kent, and A. Kaplan, 2003: Global analyses of sea surface temperature, sea ice, and night marine air temperature since the late nineteenth century. *J. Geophys. Res.,* **108,** 4407, doi:10.1029/2002JD002670.

Robel, J., cited 2009: NOAA KLM user's guide (February 2009 rev. ed.) NOAA/National Climatic Data Center, February 2009 ed. [Available online at http://www.ncdc.noaa.gov/oa/pod-guide/ncdc/docs/intro.htm.]

Saunders, R., M. Matricardi, and P. Brunel, 1999: An improved fast radiative transfer model for assimilation of satellite radiance observations. *Quart. J. Roy. Meteor. Soc.,* **125,** 1407–1425.

Sherlock, V. J., 1999: ISEM-6: Infrared surface emissivity model for RTTOV-6. Met Office Forecasting Research Tech. Rep. 299, 17 pp.

Sherwood, S. C., R. Roca, T. M. Weckwerth, and N. G. Andronova, 2010: Tropospheric water vapor, convection, and climate. *Rev. Geophys.,* **48,** RG2001, doi:10.1029/2009RG000301.

Shi, L., and J. J. Bates, 2011: Three decades of intersatellite-calibrated High-Resolution Infrared Radiation Sounder upper tropospheric water vapor. *J. Geophys. Res.,* **116,** D04108, doi:10.1029/2010JD014847.

——, ——, and C. Cao, 2008: Scene radiance–dependent inter-satellite biases of HIRS longwave channels. *J. Atmos. Oceanic Technol.,* **25,** 2219–2229.

Smith, G. L., P. E. Mlynczak, D. A. Rutan, and T. Wong, 2008: Comparison of the diurnal cycle of outgoing longwave radiation from a climate model with results from ERBE. *J. Appl. Meteor. Climatol.,* **47,** 3188–3201.

Soden, B. J., 2000: The diurnal cycle of convection, clouds, and water vapor in the tropical upper troposphere. *Geophys. Res. Lett.,* **27,** 2173–2176.

——, R. T. Wetherald, G. L. Stenchikov, and A. Robock, 2002: Global cooling after the eruption of Mount Pinatubo: A test of climate feedback by water vapor. *Science,* **296,** 727–730, doi:10.1126/science.296.5568.727.

——, D. Jackson, V. Ramaswamy, M. Schwarzkopf, and X. Huang, 2005: The radiative signature of upper tropospheric moisten-ing. *Science,* **310,** 841–844, doi:10.1126/science.1115602.

Sohn, B.-J., J. Schmetz, and E.-S. Chung, 2008: Moistening pro-cesses in the tropical upper troposphere observed from Me-teosat measurements. *J. Geophys. Res.,* **113,** D13109, doi:10.1029/2007JD009527.

Solomon, S., D. Qin, M. Manning, M. Marquis, K. Averyt, M. M. B. Tignor, H. L. Miller Jr., and Z. Chen, Eds., 2007: *Climate Change 2007: The Physical Science Basis.* Cam-bridge University Press, 996 pp.

Tian, B., B. Soden, and X. Wu, 2004: Diurnal cycle of convection, clouds, and water vapor in the tropical upper troposphere: Satellites versus a general circulation model. *J. Geophys. Res.,* **109,** D10101, doi:10.1029/2003JD004117.

Yang, G., and J. Slingo, 2001: The diurnal cycle in the tropics. *Mon. Wea. Rev.,* **129,** 784–801.

Zeng, Z., W. Randel, S. Sokolovskiy, C. Deser, Y.-H. Kuo, M. Hagan, J. Du, and W. Ward, 2008: Detection of migrating diurnal tide in the tropical upper troposphere and lower stratosphere using the Challenging Minisatellite Payload radio occultation data. *J. Geophys. Res.,* **113,** D03102, doi:10.1029/2007JD008725.